Periodic Hartree−Fock Study of Li_xTiS_2, $0 \leq x \leq 1$: The Structural, Elastic, and Electronic Effects of Lithium Intercalation in TiS_2

D. G. Clerc* and R. D. Poshusta

Materials Science Program, Washington State University, Pullman, Washington 99164-4630

A. C. Hess

Environmental Molecular Sciences Laboratory, MS K1-90, Pacific Northwest Laboratory, Richland, Washington 99352

Received: June 25, 1996; In Final Form: June 4, 1997[⊗]

The structural and electronic properties of the intercalation compound Li_xTiS_2, $x = {}^1/_4$, ${}^3/_4$, and 1, are investigated at the ab initio, all-electron, periodic Hartree−Fock level, using an extended basis set and a posteriori density functional correlation corrections to the total energy. Calculated lattice parameters, bulk moduli, linear moduli, cohesive energy, elastic constants, band structure, density of states, and Mulliken populations are reported. This study indicates that the following physical changes in Li_xTiS_2 are induced by intercalation. (1) The crystal expands uniaxially in the $\vec{c}$ direction. (2) The S−Ti−S layers expand negligibly (<0.01 Å) in the $\vec{c}$ direction at $x = {}^1/_4$, but a large (0.16 Å) layer expansion occurs at $x = 1$. (3) The elastic properties change negligibly at $x = {}^1/_4$, but the interlayer stiffness c_{33} increases by a factor of ∼4 at $x = 1$. (4) Lithium charge is donated to the S(3p) and Ti(3d) orbitals. At least 75% of this charge is acquired by sulfur atoms. (5) At $x = {}^1/_4$, the donated charge is localized over the lithium near-neighbor S(3p) and Ti(3d) orbitals. (6) Charge transfer to a Ti(3d)-based conduction band yields metallic properties.

1. Introduction

Li_xTiS_2 belongs to the family of alkali-intercalated transition metal dichalcogenides A_xMCh_2 (A = alkali metal, M = transition metal, Ch = S, Se, or Te). Several of these compounds have been extensively studied for use as cathode materials in ambient temperature high-energy density batteries.[1−3] Of these compounds, Li_xTiS_2 is the most promising because of its nearly ideal electrochemical properties.[4]

The unusual affinity of MCh_2 for intercalation is due to its characteristic bonding anisotropy. For example, in TiS_2 the Ti atoms lie in planes that are individually sandwiched between two parallel planes of hexagonally packed S atoms. The bonding within these S−Ti−S "layers" is of the strong covalent type, whereas the coupling between adjacent layers is relatively weak. Consequently, the intercalated species is inserted into the interlayer space, commonly called the van der Waals (vdW) gap, where the bonding is weaker.

The outstanding technological potential of Li_xTiS_2 has prompted many experimental studies in recent years. Electrochemical measurements show that lithium and TiS_2 react continuously and reversibly over the composition range $0 \leq x \leq 1$ to yield the single-phase product Li_xTiS_2. X-ray studies[5,6] of Li_xTiS_2 show that the original symmetry of the host is retained and that there is a continuous c-axis expanison for $0 \leq x \leq 1$. Magnetic susceptibility measurements[7] over the temperature range 4.2−300 K confirm the metallic nature of Li_xTiS_2 ($0 < x \leq 1$). In addition to being a good electronic conductor,[8] Li_xTiS_2 is also a good ionic conductor[7] due to the high mobility of the Li^+ ion in the vdW gap. ^{7}Li NMR[9] and cell-emf[10] measurements suggest that electron transfer from Li to TiS_2 is not complete above $x = 0.80$, with 10%−20% of the valence electron density remaining in the vicinity of the lithium atoms in $LiTiS_2$.[10]

This paper reports our theoretical investigation of Li_xTiS_2 which builds upon our previous ab initio study of TiS_2.[11] The results are compared to experiment and to previous theoretical studies.

2. Method of Calculation

Our calculations are performed using CRYSTAL92,[12,13] a well-documented ab initio program that has been applied to a wide range of ionic, covalent, and molecular crystals[14−20] as well as to adsorbate/surface interactions.[21] The method is an all-electron periodic Hartree−Fock (PHF) self-consistent-field (SCF) procedure that expands the ground-state wave function as a linear combination of atomic orbitals.

As is customary, the atomic orbitals are linear combinations of Gaussian functions which are collectively called the basis set. The titanium and sulfur basis sets used in this study are derived from titanium 86411+(3-1)d and sulfur 883-(1)d Gaussian functions originally optimized in TiS_2.[11] The lithium basis set was originally optimized[22] in Li_2O and is reoptimized in the ion Li^+. With the exception of core shells, the exponents and contraction coefficients of the three basis sets were subsequently reoptimized in $LiTiS_2$ by minimizing the PHF energy at the experimental geometry. The basis sets are given in Table 1.

In this study, the Fock matrix is diagonalized at 65 k points in the irreducible part of the first Brillouin zone. The Fermi energy (E_F) is computed at each SCF cycle by interpolating between the eigenvalues at 417 k points. Energy band interpolation is accomplished by fitting the bands to eight symmetrized plane waves.

The present work couples the HF approach with density functional theory to produce Li_xTiS_2 total energies which are corrected for electron correlation. This correction is important in systems having nonbonded orbitals such as the layered sulfides. The correction is obtained by integrating correlation-

[⊗] Abstract published in *Advance ACS Abstracts,* November 1, 1997.

S1089-5639(96)01878-6 CCC: $14.00

TABLE 1: $LiTiS_2$ Basis Set Gaussian Exponents (in au^{-2}) and Contraction Coefficients[a]

atom	orbital	exponent	s coefficient	p coefficient	d coefficent
Ti	4sp*°	0.7666	1.000	1.000	
	5sp*°	0.307 84	1.000	1.000	
	1d°	6.201			0.132
		1.567			0.348
		0.4614			0.425
	2d*°	0.1345			1.000
S	4sp*°	0.159 07	1.000	1.000	
	1d*°	0.3278			1.000
Li	1s	999.999 878	0.001 054		
		247.569 041	0.003 551		
		71.978 637	0.019 296		
		18.345 327	0.094 176		
		5.090 717	0.292 767		
		1.576 736	0.489 180		
	2sp°	0.529 762	1.000 000	1.000 000	

[a] Asterisks denote atomic orbitals assumed to be unoccupied at the beginning of the calculations. Circles denote exponents and coefficients optimized in $LiTiS_2$. Core orbitals (Ti(1s, 2sp, 3sp) and S(1s, 2sp, 3sp)) are given in ref 11.

only density functionals over all space using the converged HF electron density. Here we use two a posteriori correlation-only density functionals: Wigner's local correlation formula gradient-corrected following Lévy's method (WL)[23] and Perdew's generalized gradient approximation (P).[24] Results are reported as purely Hartree−Fock (HF) or as Hartree−Fock with correlation correction (WL or P).

3. Crystal Structure

The lattices of TiS_2 and $LiTiS_2$ are both defined by vectors $\vec{a}$, $\vec{b}$, and $\vec{c}$, where $|\vec{a}| = |\vec{b}|$, $\vec{a} \perp \vec{c}$, $\vec{b} \perp \vec{c}$, and $\angle(\vec{a}, \vec{b}) = 120°$. The $LiTiS_2$ experimental lattice parameters are $|\vec{a}| = 3.4590(3)$ Å, $|\vec{c}| = 6.1879(6)$ Å, and $z_s = 0.238(1)$,[25] where z_s is the fractional sulfur z-coordinate. In $LiTiS_2$, the lithium atom is positioned directly above the titanium atom as indicated by the fractional atomic coordinates Ti (0,0,0), S ($^1/_3$, $^2/_3$, z_s), S ($^2/_3$, $^1/_3$, $-z_s$), and Li (0, 0, $^1/_2$). The projection of four primitive $LiTiS_2$ unit cells onto the titanium plane ($z = 0$) is shown in Figure 1A.

The hexagonal close-packing of the sulfur atoms in TiS_2 gives rise to two types of interlayer sites for lithium occupation. Two tetrahedral sites are at ($^1/_3$, $^2/_3$, $^5/_8$) and ($^2/_3$, $^1/_3$, $^3/_8$); one octahedral site is at (0, 0, $^1/_2$). Neutron diffraction experiments show that the lithium atoms in Li_xTiS_2 occupy the octahedral sites in a disordered fashion.[25] However, intercalation does not disrupt intralayer structure because X-ray diffraction studies indicate that the symmetry of the TiS_2 sublattice ($P\bar{3}m1$) in Li_xTiS_2, $0 \le x \le 1$, is retained.[5,6]

In Li_xTiS_2, $0 < x < 1$, there is no observed periodic ordering of lithium atoms.[25] However, we necessarily employ an ordered structure so that calculations are tractable. Specifically, we define a Li_xTiS_2 supercell (S-cell) by $2\vec{a}$, $2\vec{b}$, and $\vec{c}$. Lithium atoms are then inserted into the octahedral sites to satisfy the conditions $x = 0$, $^1/_4$, $^3/_4$, or 1. The projection of a Li_xTiS_2 S-cell upon the vdW gap midplane ($z = ^1/_2$) is shown in Figure 1B.

As shown in Figure 1B, atoms in the S-cell separate into distinct sets, as required by D_{3d} point group symmetry. These sets are $\tau1 = \{Ti^{(1)}\}$, $\tau2 = \{Ti^{(2)}-Ti^{(4)}\}$, $\sigma1 = \{S^{(5)}-S^{(10)}\}$, and $\sigma2 = \{S^{(11)}-S^{(12)}\}$, where numeric atom labels correspond to those in Figure 1B. Similarly, S-cell octahedral sites separate into two sets: O1 = {(0, 0, $^1/_2$)}; O2 = {($^1/_2$, 0, $^1/_2$), (0, $^1/_2$, $^1/_2$), ($^1/_2$, $^1/_2$, $^1/_2$)}.

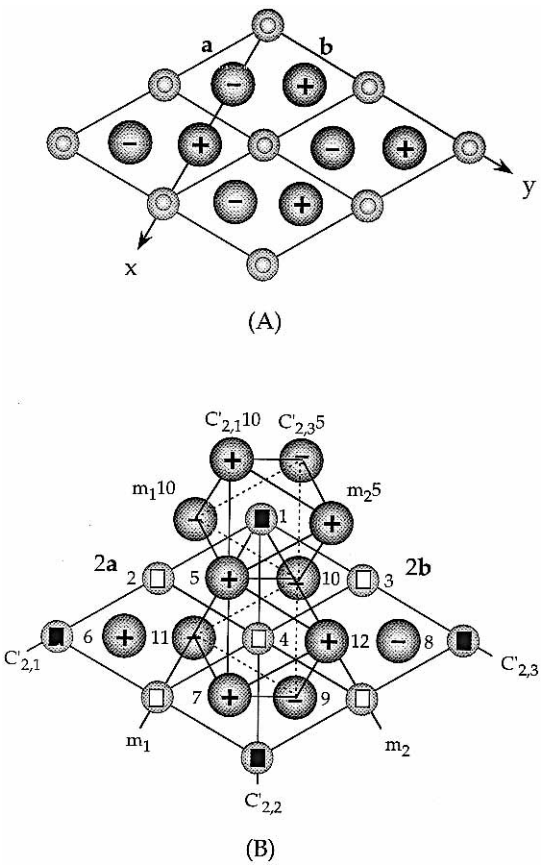

Figure 1. (A) Projection of the $LiTiS_2$ unit cell onto the Ti plane. Large + (−) spheres are S above (below) the Ti plane. Medium-sized spheres are Ti, and small spheres are Li in interlayer octahedral sites. Hexagonal lattice vectors $\vec{a}$, $\vec{b}$, and $\vec{c}$ satisfy $|\vec{a}| = |\vec{b}|$, $\vec{a} \perp \vec{c}$, $\vec{b} \perp \vec{c}$, and $\angle(\vec{a}, \vec{b}) = 120°$. (B) Projection of the Li_xTiS_2 unit cell onto the van der Waals gap midplane ($z = ^1/_2$). Large + (−) spheres are S above (below) the midplane; smaller spheres are Ti atoms. Filled (open) squares denote octahedral sites O1 (O2) that are separately occupied in $Li_{0.25}TiS_2$ ($Li_{0.75}TiS_2$). Several D_{3d} point group operators are shown: m = mirror plane, C_2' = 2-fold rotation axis. The nearest neighbor atoms of O1 are labeled by their generating symmetry operations.

There are four possible Li_xTiS_2 stoichiometries using the S-cell of Figure 1B. The trivial cases $x = 0$ and $x = 1$ correspond to TiS_2 and $LiTiS_2$, respectively, and these crystals can also be represented using a primitive cell (P-cell). When $x = ^1/_4$ and $x = ^3/_4$, lithium atoms occupy sites O1 and O2, respectively. The case $x = ^1/_2$ corresponds to lower symmetry than $P\bar{3}m1$. Because of the associated computational expense, the properties of $Li_{0.5}TiS_2$ are not investigated.

4. Computational Results

Results are presented in two sections entitled "Structural Properties" and "Electronic Properties". The notation $p^M(x)$ is used to denote property p of Li_xTiS_2 obtained using method M, where M may be HF, P, WL, or EXP (experimental). The value of $p^M(x_2)$ relative to $p^M(x_1)$ is denoted by $p^M(x_1 \rightarrow x_2) = p^M(x_2) - p^M(x_1)$.

4.1. Structural Properties. In this section, we present calculated Li_xTiS_2 equilibrium geometries, bulk moduli (B), linear moduli (B_a and B_c), stiffness constants (c_{ij}), compliance constants (s_{ij}), and cohesive energies at $x = 0$, $^1/_4$, and 1. Equilibrium geometries were computed by minimizing the total energy with respect to a, c, and z_s. The c_{ij} are the fitting coefficients that expand the total energy quadratically in terms of small displacements of the a- and c-axes. In these expansions, internal relaxation effects were computed by optimizing

TABLE 2: Structural Properties[a]

	TiS_2			$Li_{0.25}TiS_2$		$LiTiS_2$			
	P	WL	EXP	P	EXP	HF	P	WL	EXP
a (Å)	3.417(0)	3.321(1)	3.4073(2)[b]	3.409(2)	3.415[c]	3.501(0)	3.374(2)	3.250(1)	3.4590(3)[c]
c (Å)	5.990(9)	5.615(5)	5.6953(2)[b]	6.00(3)	6.04[c]	6.282(5)	6.070(4)	5.996(8)	6.1879(6)[c]
z	0.2281(20)	0.2440(27)	0.2501(4)[b]	0.2270(20)		0.2339(5)	0.2382(5)	0.2432(5)	0.238(1)[c]
$L\mathscr{T}$(Å)[a]	2.73(2)	2.74(3)	2.849(4)	2.72(3)		2.939(7)	2.892(6)	2.916(7)	2.945(12)
c-$L\mathscr{T}$(Å)	3.26(2)	2.88(3)	2.846(4)	3.28(3)		3.345(7)	3.178(6)	3.080(7)	3.243(12)
ρ (g/cm^3)[a]	3.07(1)	3.47(1)	3.285(4)	3.13(2)	3.10	2.963(2)	3.302(4)	3.602(5)	3.0810(6)
B (GPa)	34(3)	42(4)	41[d]	27(8)		91(1)	103(1)	116(8)	
B_a (GPa)	314(9)	311(21)	179[e], 260[d]	269(25)	227[f]	302(5)	357(6)	384(24)	
B_c (GPa)	44(5)	58(6)	59[e], 61[d]	34(12)	65[f]	230(5)	242(7)	295(17)	
$c_{11}+c_{12}$ (GPa)	271(2)	263(3)	202[g]	273(9)		262(5)	295(7)	323(9)	
c_{13} (GPa)	6(1)	31(3)	14[g]	0(3)		29(3)	42(4)	47(3)	
c_{33} (GPa)	42(4)	55(5)	55(5)[h]	34(12)		183(2)	185(1)	222(14)	
$s_{11}+s_{12}$ (GPa^{-1})	0.00371(3)	0.00385(4)	0.00513[g]	0.00367(13)		0.00398(11)	0.00364(15)	0.00331(6)	
s_{13} (GPa^{-1})	−0.00054(9)	−0.00064(19)	−0.0013[g]	0.0001(3)		−0.00067(10)	−0.00083(11)	−0.00071(6)	
s_{33} (GPa^{-1})	0.024(2)	0.019(1)	0.019[g]	0.0326(10)		0.00570(13)	0.00580(11)	0.00481(30)	
$\Delta E°_{coh,0K}$ (kcal/mol)[i]	398(5)	474(5)	340(1)	453(5)		465(5)	605(5)	701(5)	

[a] $L\mathscr{T} = 2cz_s$, ρ = density. [b] From ref 26. [c] 300 K values from ref 25, Figure 6. [d] From ref 27. [e] From ref 28. [f] $Li_{0.50}TiS_2$ value from ref 28. [g] Calculated from experimental values of B_a, B_c, and c_{33}. [h] From ref 29. [i] See Table 4 for calculation.

all symmetry-independent atomic coordinates at each displacement. The $LiTiS_2$ and $Li_{0.25}TiS_2$ results were obtained using the P-cell and S-cell, respectively.

4.1.1. Lattice Parameters. The calculated equilibrium Li_x-TiS_2 geometries and layer thickness $L\mathscr{T}$ ($L\mathscr{T} = 2cz_s$) are presented in Table 2 with the available experimental data.

As was the case for TiS_2, correlation corrections are required to bind $Li_{0.25}TiS_2$ in the $\vec{c}$ direction.[11] The P results for the a-axis and c-axis are 3.409(2) and 6.00(3) Å, respectively. The corresponding differences with experiment are only −0.2% and 0.7%.

In $LiTiS_2$, the HF approach binds the crystal in the $\vec{c}$ direction, unlike the $x = 0$ and $x = 0.25$ cases. Furthermore, the HF and P lattice parameters of $LiTiS_2$ are within ∼3.6%. The WL a- and c-axes, on the other hand, are underestimated slightly by 6.0% and 3.1%, respectively. For $LiTiS_2$, the differences between our results and experiment—in the order HF, P, WL—are 1.2%, −2.4%, and −6.0% for the a-axis; 1.5%, −1.9%, and −3.1% for the c-axis; and −1.7%, 0.08%, and 2.2% for z_s.

As shown in Table 2, the calculated lattice parameters at $x = 0$, $^1/_4$, and 1 reveal two important effects of intercalation. (1) $L\mathscr{T}$ exhibits negligible change at $x = {}^1/_4$, whereas a large increase occurs at $x = 1$. (2) A nearly uniaxial expansion occurs in the $\vec{c}$ direction.

The calculated $L\mathscr{T}$s suggest that the layers expand only when sufficient ($x > {}^1/_4$) lithium is intercalated. Specifically, $L\mathscr{T}^{\mathrm{P}}(0 \rightarrow {}^1/_4) = -0.008$ Å, whereas $L\mathscr{T}^{\mathrm{P}}(0 \rightarrow 1) = +0.16$ Å. The large increase in $L\mathscr{T}^{\mathrm{P}}$ at $x = 1$ is similar to $L\mathscr{T}^{\mathrm{WL}}(0 \rightarrow 1) = +0.18$ Å and $L\mathscr{T}^{\mathrm{EXP}}(0 \rightarrow 1) = +0.10$ Å.

The computed crystal expansion is essentially uniaxial in the $\vec{c}$ direction. Specifically, $c^{\mathrm{WL}}(0 \rightarrow 1) = +0.38$ Å and $a^{\mathrm{WL}}(0 \rightarrow 1) = -0.07$ Å, which is similar to experiment: $c^{\mathrm{EXP}}(0 \rightarrow 1) = +0.49$ Å and $a^{\mathrm{EXP}}(0 \rightarrow 1) = +0.05$ Å. In the P approach, however, the c-axis expansion $c^{\mathrm{P}}(0 \rightarrow 1) = 0.08$ Å is much smaller due to the large (6%) overestimation of $c^{\mathrm{P}}(0)$. Both schemes yield small a-axis contractions: $a^{\mathrm{P}}(0 \rightarrow 1) = -0.04$ Å and $a^{\mathrm{WL}}(0 \rightarrow 1) = -0.07$ Å, in disagreement with the small experimentally observed expansion $a^{\mathrm{EXP}}(0 \rightarrow 1) = 0.05$ Å.

4.1.2. Elastic Properties. Elastic properties are used herein to quantify the crystalline bonding strength or stiffness in specific directions. For example, the stiffnesses in the $\vec{c}$ direction, in directions parallel to the ab plane, and in linear combinations of these directions are c_{33}, $c_{11}+c_{12}$, and c_{13} respectively.

Inspection of Table 2 indicates that at $x = 1$ a marked stiffening in the $\vec{c}$ direction occurs with a dramatic reduction of bonding anisotropy relative to results at $x = 0$ and $x = {}^1/_4$. The interlayer stiffening follows from $c_{33}^{\mathrm{P}}(1)/c_{33}^{\mathrm{P}}(0) \approx 4$ and $B_c^{\mathrm{P}}(1)/B_c^{\mathrm{P}}(0) \approx 5$. The reduction of bonding anisotropy at $x = 1$ is evidenced by $c_{11}+c_{12}^{\mathrm{P}}(1)/c_{33}^{\mathrm{P}}(1) = 1.59$, whereas $c_{11}+c_{12}^{\mathrm{P}}(0)/c_{33}^{\mathrm{P}}(0) = 6.45$. Differences in intralayer stiffness are relatively small since $B_a^{\mathrm{P}}(1)/B_a^{\mathrm{P}}(0) = 1.18$ and $c_{11}+c_{12}^{\mathrm{P}}(1)/c_{11}+c_{12}^{\mathrm{P}}(0) = 1.16$. As seen in Table 2, the c_{ij} at $x = {}^1/_4$ and $x = 0$ are similar, which suggests that the said $LiTiS_2$ elastic properties are induced by intercalation when $^1/_4 < x \leq 1$.

The predicted invariance of c_{33} when $x \leq 0.25$ ($c_{33}^{\mathrm{P}}(0 \rightarrow 0.25) = -8$ GPa) suggests that the presence of the lithium ion in one-fourth of the interlayer sites does not appreciably alter the strength of bonding across the vdW gap. This assertion is further supported by the inability of HF to bind TiS_2 and $Li_{0.25}$-TiS_2 in the $\vec{c}$ direction, which suggests that some degree of weak vdW-type bonding exists in the interlayer space of both compounds.

The ability of the HF method to bind Li_xTiS_2 at $x = 1$ but not when $x \leq {}^1/_4$ provides valuable insights into the relative types of bonding. Evidently, the weaker vdW-type bonding in TiS_2 and $Li_{0.25}TiS_2$ is replaced by the stronger ionic bonding in $LiTiS_2$, which is more accurately treated using the HF approximation. This assertion is supported by the trend $c_{33}^{\mathrm{P}}(0) \approx c_{33}^{\mathrm{P}}(0.25) \ll c_{33}^{\mathrm{P}}(1)$ and by Mulliken populations (discussed below).

4.1.3. Cohesive Energy. The cohesive energy is the difference between the total energy of the crystal at equilibrium and the total energies of the isolated atomic components. However, the inverse (negative) definition is used below so that cohesive energies appear positive. Calculated values of the Li_xTiS_2 cohesive energy at 0 K, $\Delta E_{coh,0K}$, are shown in Table 2. Computational details appear in Table 3.

The cohesive energies in Table 2 are consistent with continuous and reversible intercalation. As seen in the table, the cohesive energy per lithium atom at $x = {}^1/_4$ is not significantly different from that at $x = 1$. Specifically, $4\Delta E_{coh,0K}^{\mathrm{P}}(0 \rightarrow {}^1/_4) = 220(5)$ kcal/mol $\approx \Delta E_{coh,0K}^{\mathrm{P}}(0 \rightarrow 1) = 207(5)$ kcal/mol. A significantly lower cohesive energy at $x = {}^1/_4$ would indicate that filling one-fourth of the vdW gap sites is energetically favorable relative to complete intercalation. However, the resulting similar cohesive energies is consistent with the observed continuous reversible filling of the vdW gap over the composition range $0 \leq x \leq 1$.

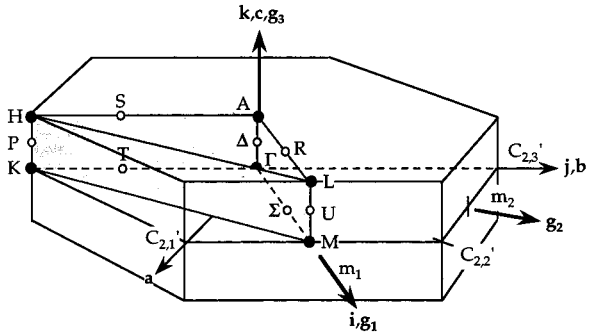

Brillouin zone of Li_xTiS_2, $0 \le x \le 1$

Direct lattice vectors
a=(3^1/2/2)**ai** - (1/2)**aj**
b=**aj**
c=**ck**

Reciprocal lattice vectors
$g_1=(4\pi/3^{1/2}a)\mathbf{i}$
$g_2=(2\pi/3^{1/2}a)(\mathbf{i}+3^{1/2}\mathbf{j})$
$g_3=(2\pi/c)\mathbf{k}$

k point coordinates & point symmetry
Γ = (0, 0, 0), D_{3d}
M = (1/2, 0, 0), C_{2h}
K = (1/3, -2/3, 0), D_3
A = (0, 0, 1/2), D_{3d}
L = (1/2, 0, 1/2), C_{2h}
H = (1/3, -2/3, 1/2), D_3
Δ: C_{3v}
Σ, R, U: C_s
S, T: C_2
P: C_3

Figure 2. First Brillouin zone of Li_xTiS_2, $0 \le x \le 1$. Cartesian unit vectors ($\hat{i}$, $\hat{j}$, and $\hat{k}$), direct lattice vectors ($\vec{a}$, $\vec{b}$, and $\vec{c}$), and reciprocal lattice vectors ($\vec{g}_1$, $\vec{g}_2$, and $\vec{g}_3$) are shown. The perimeter of the shaded planes corresponds to the segments given in the electronic band structure. Also shown are the Cartesian representations of the direct and reciprocal lattice vectors as well as the $\vec{k}$ point reciprocal lattice coordinates and their associated point groups in Schöenflies notation.

4.2. Electronic Properties. In this section, we report the Li_xTiS_2 electronic band structures, total densities of states (DOS), projected densities of states (PDOS), and Mulliken populations. The first Brillouin zone for the hexagonal lattice of Li_xTiS_2 is depicted in Figure 2 following the notation of Bradley and Cracknell.[30] The set of $\vec{k}$ points used in computing the energy bands and their associated point groups in Schöenflies' notation are also shown.

In the following discussion, the energy zero for all materials is the TiS_2 Fermi energy, the energy of the highest energy occupied TiS_2 eigenstate. The Fermi energies (E_F) of each material are denoted by dashed lines in band structure plots, and the energy of the nth band at $\vec{k}$ is denoted by $\epsilon(\vec{k})_n$. Band structures are reported using the same size Brillouin zone for each material. Last, numeric band labels refer to the eigenvalue order rather than symmetry. For example, degenerate bands 26 and 27, $\epsilon(\vec{k})_{26-27}$, are the highest energy occupied TiS_2 eigenstates since there are 54 electrons per TiS_2 formula unit.

4.2.1. Electronic Band Structure. The TiS_2 and $LiTiS_2$ energy bands are compared in Figure 3A, where many similarities are apparent. In particular, bands are grouped into distinct sets including six valence bands (VB1) directly below E_F, two valence bands (VB2) below VB1, and five conduction bands (CB1) above VB1. Lithium intercalation does not generate any new bands in VB2, VB1, or CB1.

The TiS_2 and $LiTiS_2$ band topologies are similar to those from previously reported band structures. The TiS_2 energy bands closely resemble those from Xα exchange fitted-free-electron-correlation density functional theory,[31] Green's function theory (KKR),[32] and those of Umrigar et al. computed using the self-consistent linearized augmented plane wave method (SC-LAPW).[33] The $LiTiS_2$ band topology is also similar to that Umrigar et al.[34] However, in both TiS_2 and $LiTiS_2$, we observe

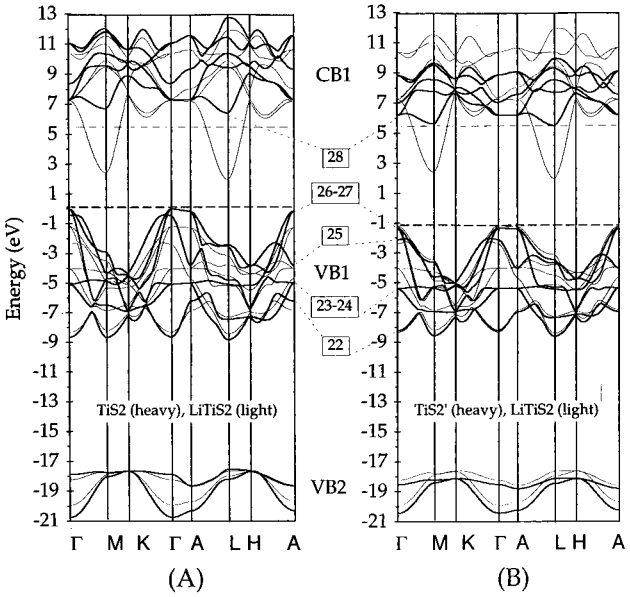

Figure 3. (A) Hartree−Fock P-cell electronic band structures of $LiTiS_2$ (light lines) with (A) TiS_2 (heavy lines), and (B) TiS_2' (heavy lines). Brillouin zone segments are defined in Figure 2. The dashed lines are at the Fermi energies (highest energy occupied eigenstate). Band labels correspond to the eigenvalue order in TiS_2 (see text). The ordinate zero is the TiS_2 Fermi energy.

overestimations of the energy gaps and bandwidths that are typical of Hartree−Fock.

The differences between the $LiTiS_2$ and TiS_2 energy bands in Figure 3A can be attributed to (1) lattice expansion and (2) chemical reduction. These two effects are differentiated by comparing energy bands to those of TiS_2', where TiS_2' is a TiS_2 crystal expanded to the same unit cell dimensions as $LiTiS_2$.

The effects of lattice expansion are discerned by comparing the TiS_2 (Figure 3A) and TiS_2' (Figure 3B) energy bands. These effects include (1) a 1 eV downward shift of the five highest energy valence bands on Γ−A; (2) a 1 eV decrease in the VB1 bandwidth; and (3) a 0.5 eV increase in the energy gap between S(3p)-based bands $\epsilon(\Gamma)_{25}$ and $\epsilon(\Gamma)_{26-27}$. These three effects are due to the S(3p)-based band sensitivity to the distance across the van der Waals gap.[11]

The effects of chemical reduction are evident in Figure 3B, where the $LiTiS_2$ and TiS_2' energy bands are superimposed. These effects are (1) metallicity and (2) a 1 eV shift of $\epsilon(\Gamma-A)_{23-24}$ toward E_F. This shift occurs when $0.25 \le x \le 0.75$ and its causes are speculated upon in a later section.

Analysis of the eigenvector composition of the lowest energy $Li_{0.25}TiS_2$ CB1 band, $\epsilon(L)_{28}$, suggests that the Ti($3d_{z^2}$) orbital nearest O1 accepts charge at small x to induce metallicity. Specifically, at $x = 0.25$ only the Ti$(3d_{z^2})^{r_1}$ and Ti$(3\delta)^{r_2}$ orbitals contribute to $\epsilon(L)_{28}$, where Ti$(3\delta) \equiv$ Ti($3d_{xz}$, $3d_{yz}$, $3d_{x^2-y^2}$, $3d_{xy}$). Since the Ti$(3d_{z^2})^{r_1}$ orbital is closer to the lithium atom, charge transfer to Ti$(3d_{z^2})^{r_1}$-based CB1 crystal orbitals likely induces metallic properties at earlier ($x < 0.25$) stages of intercalation.

4.2.2. Density of States. In this section we contrast the TiS_2 and $LiTiS_2$ DOS. The calculated VB1 DOS features follow the TiS_2 notation of Shephard and Williams[34] including subscript "c" (a_c, α_c, β_c, γ_c, and δ_c). The DOS and PDOS of TiS_2 and $LiTiS_2$ are shown in Figure 4.

As seen in Figure 4, VB1 in both materials derives mainly from S(3p) orbitals, and a Ti(3d) contribution occurs at peak β_c. Similarly, VB2 derives from S(3s) orbitals, and the lower energy states in CB1 assign to Ti(3d) orbitals.

Inspection and comparison of Figure 4 to the energy bands (Figure 3) show that complete intercalation has four significant

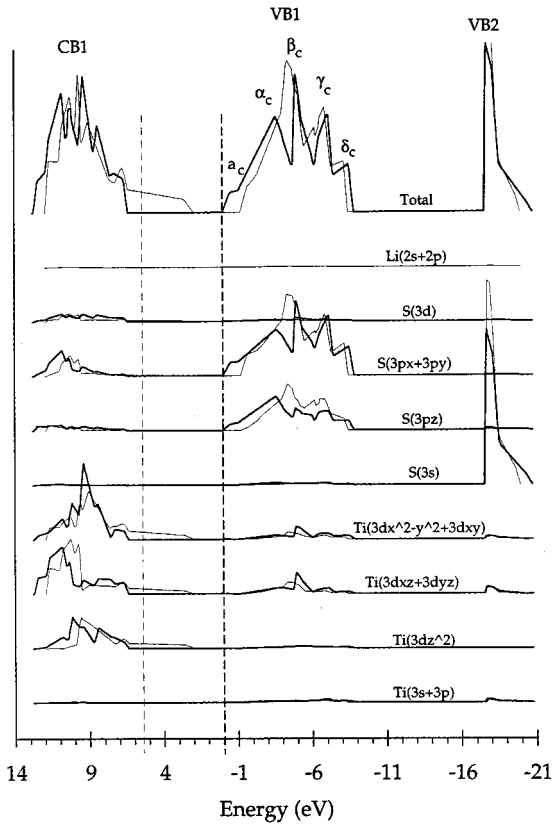

Figure 4. Hartree−Fock 1-cell DOS and PDOS of TiS_2 (heavy lines) and $LiTiS_2$ (light lines). The dashed lines are at the Fermi energies (highest energy occupied eigenstate). Orbital labels are defined in Table 4, and VB1 features are labeled following ref 34.

effects upon the DOS. Lattice expansion accounts for two effects: (1) a 1 eV decrease in the VB1 bandwidth; (2) a dramatic reduction in the S($3p_z$) contribution to peak a_c. Chemical reduction accounts for the two remaining effects: (3) metallicity; (4) the merging of peaks α_c and β_c due to the shift of $\epsilon(\Gamma-A)_{23-24}$ and hence peak β_c toward E_F by 1 eV.

The S-cell Li_xTiS_2 density of states at $x = 0$, $^1/_4$, $^3/_4$, and 1 (not shown) shows that peak β_c moves toward peak α_c only when $x > 0.25$. This result suggests that a critical amount of intercalation is required to initiate the shift of peak β_c.

4.2.3. Mulliken Population. Mulliken population analyses are used in this study as rough indicators of intercalation-induced charge rearrangements. The Li_xTiS_2 Mulliken populations are given in Table 4.

As seen in Table 4, there are two significant charge rearrangements which accompany lithium intercalation. (1) 75% or more of the Li(2s) electron is transferred to S(3p) orbitals, whereas the remainder is transferred to Ti(3d) orbitals. (2) At $x = {}^1/_4$, charge transferred from the lithium atom is localized over the O1 near-neighbor orbitals $S(3p)^{\sigma_1}$ and $Ti(3d)^{\tau_1}$.

Our $LiTiS_2$ results are consistent with those of Umrigar et al.,[34] where the SC-LAPW approach was used to investigate the electronic properties of TiS_2 and $LiTiS_2$. Their results indicate that charge shifts away from the Ti plane at $x = 1$ despite charge donation to a Ti(3d)-based crystal orbital. Furthermore, the charge density increase was found to lie primarily between the Li and S planes. Consistent with this, our results indicate that $0.37|e|$ is donated to each S atom, whereas a smaller amount, $0.23|e|$, goes to each Ti atom. Furthermore, the layers become more ionic because the amount of charge participating in titanium−sulfur bonding is $0.75|e|$ lower at $x = 1$ that at $x = 0$.

TABLE 3: Cohesive Energy Calculations[a]

	HF	HF+P	HF+WL
$x = 1$			
E(Ti)[b] (au)	−848.138	−849.074	−849.073
E(S)[b] (au)	−397.489	−398.136	−398.147
E(Li) (au)	−7.187	−7.248	−7.237
E(Ti) + 2E(S) + E(Li) (au)	−1650.303	−1652.594	−1652.604
$E(LiTiS_2)$ (au)	−1651.045	−1653.558	−1653.721
$\Delta E°_{coh,0K}$ (au)	0.742	0.964	1.117
$\Delta E°_{coh,0K}$ (kcal/mol)	465	605	701
$x = 0.25$			
E(Ti) + 2E(S) + 0.25E(Li) (au)	−1644.913	−1647.158	
$E(Li_{0.25}TiS_2)$ (au)	−1645.438[c]	−1647.880	
$\Delta E°_{coh,0K}$ (au)	0.525	0.722	
$\Delta E°_{coh,0K}$ (kcal/mol)	329	453	

[a] Zero Kelvin values: $\Delta E°_{coh,0K} = E(Ti) + 2E(S) + xE(Li) - E(Li_xTiS_2)$. [b] Atomic energies are from CRYSTAL calculations using the basis set in Table 1 with the titanium 4sp*, 5sp*, 1d, 2d*, sulfur 3sp, 4sp*, 1d*, and lithium 2sp exponents optimized in the atom. [c] Taken as the HF energy occurring at the HF+P geometry listed in Table 2.

TABLE 4: Mulliken Orbital Populations[a,b]

orbital	TiS_2	$Li_{0.25}TiS_2$[d]	$Li_{0.75}TiS_2$[d,e]	$LiTiS_2$
Ti (core)[f]	18.26	$0.00^{\tau 1}$, $0.01^{\tau 2}$	$0.01^{\tau 1}$, $0.00^{\tau 2}$	−0.03
Ti (3d)[c]	1.90	$0.11^{\tau 1}$, $0.01^{\tau 2}$	$0.10^{\tau 1}$, $0.20^{\tau 2}$	0.25
$3d_{z^2}$	0.20	$0.11^{\tau 1}$, $0.04^{\tau 2}$	$0.15^{\tau 1}$, $0.19^{\tau 2}$	0.25
3δ[c]	1.70	$0.00^{\tau 1}$, $-0.03^{\tau 2}$	$-0.05^{\tau 1}$, $0.01^{\tau 2}$	0.04
S (core)[f]	12.07	$-0.02^{\sigma 1}$, $0.00^{\sigma 2}$	$-0.03^{\sigma 1}$, $-0.04^{\sigma 2}$	−0.04
S (3p)[c]	4.85	$0.14^{\sigma 1}$, $0.02^{\sigma 2}$	$0.27^{\sigma 1}$, $0.39^{\sigma 2}$	0.40
$3p_x+3p_{xy}$	3.22	$0.07^{\sigma 1}$, $0.00^{\sigma 2}$	$0.16^{\sigma 1}$, $0.23^{\sigma 2}$	0.24
$3p_z$	1.64	$0.07^{\sigma 1}$, $0.02^{\sigma 2}$	$0.11^{\sigma 1}$, $0.16^{\sigma 2}$	0.16
Ti(tot)	20.16	$0.11^{\tau 1}$, $0.02^{\tau 2}$	$0.11^{\tau 1}$, $0.20^{\tau 2}$	0.23
S(tot)	16.92	$0.13^{\sigma 1}$, $0.01^{\sigma 2}$	$0.24^{\sigma 1}$, $0.35^{\sigma 2}$	0.37
Li(tot)	(3.00)	−0.96	−0.96	−0.96

[a] All Mulliken populations calculated using S-cell and reported in units of $|e|$. [b] Orbital populations at $x \neq 0$ are reported as MP($0 \rightarrow x$). [c] Ti(3d) = 1d + 2d titanium orbitals in Table 1. Ti(3δ) = $Ti(3d_{xz}+3d_{yz}+3d_{x^2-y^2}+3d_{xy})$. S(3p) = 3p + 4p sulfur orbitals in Table 1. [d] $\tau 1 = Ti^{(1)}$, $\tau 2 = Ti^{(2-4)}$; $\sigma 1 = S^{(5-10)}$, $\sigma 2 = S^{(11-12)}$, O1 = (0, 0, $^1/_2$), and O2 = {($^1/_2$, 0, $^1/_2$), (0, $^1/_2$, $^1/_2$), ($^1/_2$, $^1/_2$, $^1/_2$)}, where atom labels and coordinates correspond to those in Figure 1B. [e] The $x = 0.75$ results were calculated at the experimental geometry: $2a = 6.876$ Å, $c = 6.180$ Å, $z_s = 0.238$.[25] [f] Ti(core) = Ti(1s+2sp+3sp+4sp+5sp); S(core) = S(1s+2sp+3s+1d+4s).

4.3. Discussion and Speculation. Evidently, the following physical changes occur when $^1/_4 < x \leq 1$: (1) $L\mathcal{T}$ increases by ~0.16 Å, (2) c_{33} increases by a factor of ~4, and (3) $\epsilon(\Gamma-A)_{23-24}$ shifts toward E_F by 1 eV, which merges peaks α_c and β_c. To rigorously relate these phenomena, we require expectation values of the band-projected Coulomb, exchange, and kinetic energy operators. Because these quantities are unavailable in CRYSTAL92, the following speculation is used to interpret the physical changes that cause these results.

When $x \leq {}^1/_4$, electron transfer to the S(3p) orbitals may increase the layer−layer electrostatic repulsion and cause the *c*-axis to expand by a large amount. Our results at $x = {}^1/_4$ indicate that the number of intercalated Li^+ ions is insufficient to strengthen the interlayer bonding, and c_{33} remains practically unchanged. This weak bonding more easily permits a large *c*-axis expansion.

Evidently, when x increases from $^1/_4$ to 1 the intercalated lithium ions pin the layers together with increasing strength, presumably by increased electrostatic attraction. Consequently, the *c*-axis expansion diminishes, whereas c_{33} dramatically increases. Furthermore, the Ti(3d) and S(3p) populations increase, which likely raises the electrostatic repulsion between

the Ti and S planes. This increased repulsion presumably (1) forces the Ti and S planes apart, thus increasing $L\mathcal{T}$, and (2) raises the energy of $\epsilon(\Gamma-A)_{23-24}$ thus shifting it and peak β_c toward E_F.

5. Conclusions

The Li_xTiS_2 elastic properties, $L\mathcal{T}$, and $\epsilon(\Gamma-A)_{23-24}$ position change negligibly when x increases from 0 to $^1/_4$. When x increases from $^1/_4$ to 1, c_{33} increases by a factor of ∼4, $L\mathcal{T}$ increases by ∼0.16 Å, and $\epsilon(\Gamma-A)_{23-24}$ is shifted toward E_F by 1 eV.

This study also indicates the following. (1) Post-SCF correlation corrections are required to bind layers in the $\vec{c}$ direction at $x = 0$ and $x = {}^1/_4$, but not at $x = 1$. (2) In $LiTiS_2$, Perdew correlation-corrected lattice parameters are 1.2%−3.6% closer to experiment than those obtained using the Wigner−Lévy approach. However, lack of experimental data precludes similar comparison of elastic properties. (3) Li(2s) charge is donated to the Ti(3d) and S(3p) orbitals, with 75% or more distributed on the sulfur atoms. (4) The donated Li(2s) charge is localized over the O1 near-neighbor orbitals $S(3p)^{\sigma_1}$ and $Ti(3d)^{\tau_1}$. (5) Charge transfer to the $Ti(3d_{z^2})$ orbital nearest the Li atom induces metallicity at $x = {}^1/_4$. (6) Intercalation-induced lattice expansion reduces the VB1 bandwidth. (7) Intercalation-induced chemical reduction results in (a) charge transfer to $\epsilon(\vec{k})_{28}$ (hence metallicity); (b) the shift of $\epsilon(\Gamma-A)_{23-24}$ toward E_F by 1 eV when $x > {}^1/_4$; and (c) the merging of peaks α_c and β_c at $x > {}^1/_4$.

Acknowledgment. The authors are grateful for helpful discussions with Edoardo Aprà. This work was supported by the Associated Western University, Inc., Northwest (AWU NW) Laboratory Graduate fellowship, and the research was carried out at Pacific Northwest National Laboratories. The authors would also like to acknowledge the Office of Energy and Efficiency, Advanced Industrial Concepts Division, and the National Energy Research Supercomputing Center (NERSC). Pacific Northwest National Laboratory is operated for the U.S. Department of Energy by Battelle Memorial Institute under Contract No. DE-AC06-76RLO1830.

References and Notes

(1) Imanishi, N.; Toyoda, M.; Takeda, Y.; Yamamoto, O. *Solid State Ionics* **1992**, *58*, 333.
(2) Julien, C.; Sekine, T.; Balkanski, M. *Solid State Ionics* **1991**, *48*, 225.
(3) McKelvy, M. J.; Glaunsinger, W. S. *J. Solid State Chem.* **1987**, *67*, 142.
(4) Scrosati, B., Magistris, A., Mari, C. M., Mariotto, G., Eds. *Fast Ion Transport in Solids NATO ASI Series, Series E: Applied Sciences*; 1993; Vol. 250.
(5) Whittingham, M. S. *Electrochem. Soc.* **1975**, *122*, 70C.
(6) Whittingham, M. S. *Electrochem. Soc.* **1976**, *123*, 315.
(7) Bernard, L.; Glaunsinger, W.; Colombet, P. *Solid State Ionics* **1985**, *17*, 81.
(8) Julien, C.; Samaras, I.; Gorochov, O.; Ghorayeb, A. M. *Phys. Rev. B* **1992**, *45* (23), 13390.
(9) Kleinberg, R. L.; Silbernagel, B. G. *Solid State Commun.* **1980**, *36*, 345.
(10) Whittingham, M. S. *J. Solid State Chem.* **1979**, *29*, 303.
(11) Clerc, D. G.; Poshusta, R. D.; Hess, A. C. *J. Phys. Chem.* **1996**, *100* (39), 15735.
(12) Dovesi, R.; Saunders, V. R.; Roetti, C. *CRYSTAL92, An ab initio Hartree−Fock LCAO program for periodic systems*; 1992.
(13) Pisani, C.; Dovesi, R.; Roetti, C. *Hartree−Fock Ab Initio Treatment of Crystalline Systems*; Springer-Verlag: Berlin, 1988.
(14) Causà, M.; Dovesi, R.; Pisani, C.; Roetti, C. *Phys. Rev. B* **1986**, *33*, 1308.
(15) Dovesi, R.; Ermondi, C.; Ferrero, E.; Pisani, C.; Roetti, C. *Phys. Rev. B* **1984**, *29*, 3591.
(16) Causà, M.; Dovesi, R.; Roetti, C.; Kotomin, E.; Saunders, V. R. *Chem. Phys. Lett.* **1987**, *140*, 120.
(17) Dovesi, R.; Pisani, C.; Roetti, C. *J. Chem. Phys.* **1987**, *86*, 6967.
(18) Catti, M.; Pavese, A.; Dovesi, R.; Roetti, C.; Causà, M. *Phys. Rev. B* **1991**, *44*, 3509.
(19) Hess, A. C.; Saunders, V. R. *J. Phys. Chem.* **1992**, *96*, 4367.
(20) Dovesi, R.; Causà, M.; Orlando, R.; Roetti, C.; Saunders, V. R. *J. Chem. Phys.* **1990**, *92*, 7402.
(21) McCarthy, M. I.; Hess, A. C. *J. Chem. Phys.* **1992**, *96*, 6010.
(22) Dovesi, R. *Solid State Commun.* **1985**, *54* (2), 183.
(23) Wilson, L. C.; Lévy, M. *Phys. Rev. B* **1990**, *41* (18), 12930.
(24) Perdew, J. P.; Wang, Y. *Phys. Rev. B* **1991**, *45*, 13244.
(25) Dahn, J. R.; McKinnon, W. R.; Haering, R. R.; Buyers, W. J. L.; Powell, B. M. *Can. J. Phys.* **1980**, *58*, 207.
(26) Chianelli, R. R.; Scanlon, J. C.; Thompson, A. H. *Mater. Res. Bull.* **1975**, *10*, 1379.
(27) Negishi, H.; Ohara, S.; Inoue, M. *Phys. Status Solidi (b)* **1989**, *151*, 441.
(28) Zhou, O.; Fischer, J. E.; Liang, K. S. *Phys. Rev. B* **1991**, *44* (14), 7243.
(29) Schärli, M.; Lévy, F. *Phys. Rev. B* **1986**, *33* (6), 4317.
(30) Bradley, C. J.; Cracknell, A. P. *The Mathematical Theory of Symmetry in Solids*; Clarendon Press: Oxford 1972; p 107.
(31) Zunger, A.; Freeman, A. J. *Phys Rev. B* **1977**, *16* (2), 906.
(32) Myron, H. W.; Freeman, A. J. *Phys. Rev. B* **1974**, *9* (2), 481.
(33) Umrigar, C.; Ellis, D. E.; Wang, D.-s.; Krakauer, H.; Posternak, M. *Phys. Rev. B* **1982**, *26* (9), 4935.
(34) Shephard, F. R.; Williams, P. M. *J. Phys. C: Solid State Phys.* **1974**, *7*, 4416.